Accelerated warming of the Southern Ocean and its impacts on the hydrological cycle and sea ice

Jiping Liu[1] and Judith A. Curry

School of Earth and Atmospheric Sciences, Georgia Institute of Technology, Atlanta, GA 30332

Edited by Mark H. Thiemens, University of California at San Diego, La Jolla, CA, and approved July 13, 2010 (received for review March 15, 2010)

The observed sea surface temperature in the Southern Ocean shows a substantial warming trend for the second half of the 20th century. Associated with the warming, there has been an enhanced atmospheric hydrological cycle in the Southern Ocean that results in an increase of the Antarctic sea ice for the past three decades through the reduced upward ocean heat transport and increased snowfall. The simulated sea surface temperature variability from two global coupled climate models for the second half of the 20th century is dominated by natural internal variability associated with the Antarctic Oscillation, suggesting that the models' internal variability is too strong, leading to a response to anthropogenic forcing that is too weak. With increased loading of greenhouse gases in the atmosphere through the 21st century, the models show an accelerated warming in the Southern Ocean, and indicate that anthropogenic forcing exceeds natural internal variability. The increased heating from below (ocean) and above (atmosphere) and increased liquid precipitation associated with the enhanced hydrological cycle results in a projected decline of the Antarctic sea ice.

sea surface temperature | precipitation | Antarctic sea ice

The Southern Ocean plays an important role in the Earth's climate system (1). The Southern Ocean is a significant sink for heat and CO_2, the world's most biologically productive ocean, and a site for the production of the coldest, densest water that is one of the dominant driving forces for the global overturning circulation. The strong westerly winds over the Southern Ocean drive the world's largest current system, the Antarctic Circumpolar Current (ACC, with a transport of ~135 Sv), which is the crossroads of the global ocean's water masses, connecting the Atlantic, Pacific, and Indian Oceans as well as connecting the deep ocean to the surface.

Although the Southern Ocean is critical to the Earth's climate system, detailed analyses of sea surface temperature (SST) variability have been hampered by limited observations (2–4). Comparisons of temperature profiles collected during the 1990s with profiles collected starting in the 1930s that were obtained from both ship-based hydrographic surveys and autonomous floats show that the upper 1,000 m of the Southern Hemisphere Ocean has warmed substantially (~0.2 °C) during this time period, and that the warming is concentrated within the ACC (4). Modeling studies also indicate that the Southern Ocean might be undergoing rapid climate change. Climate model simulations of the National Center for Atmospheric Research (NCAR) for the 20th century that include anthropogenic forcing result in more rapid increases in SST and barotropic transport within the ACC in the south Atlantic, relative to the subtropical gyres to the north (5). If volcanic aerosols are not included, the simulated Southern Ocean warming in the climate model of the Canadian Centre for Climate Modeling and Analysis is nearly doubled, implying that the human impact on Southern Ocean warming is only partially realized at present (6).

In this study, we investigate the evolution of the spatial and temporal SST variability in the Southern Ocean using both observations and model simulations, and its impacts on the regional hydrological cycle and sea ice. The observed SST datasets used here include the Hadley Centre Sea Ice and Sea Surface Temperature (HadISST) (7), and the extended reconstructed sea surface temperature (ERSST) (8). We confine the analysis to the period 1950–1999 due to large uncertainty associated with sparse in situ SST samplings in the Southern Hemisphere for the first half of the 20th century (9).

To increase confidence in the interpretation of simulated SST variability, we restrict our analysis to models that perform well in simulating the Southern Ocean climate: (*i*) the NCAR Community Climate System Model 3.0 (CCSM3), because the observed Antarctic Oscillation and sea ice variability is well represented in CCSM3 (10, 11), and (*ii*) the Geophysical Fluid Dynamics Laboratory Coupled Climate Model (GFDL-CM2.1), which has peak winds close to the observed latitude and a reasonable wind stress over the Southern Ocean, fed with the right amount and properties of the North Atlantic Deep Water, resulting in near-observed ACC transport (12). The experiments used here include: the preindustrial control experiment (PIcntrl), the climate of the 20th century experiment (20C3M), and the 21st century climate projection experiments.

Results

Empirical Orthogonal Function (EOF) analyses performed on the area-weighted annual-mean observed SST south of 40 °S for 1950–1999 show the first EOF mode of HadISST (Fig. 1*A*) having positive values extending from middle to high latitudes of the Southern Ocean, and negative values in the Antarctic and sub-Antarctic zones. The corresponding principle component (PC) (Fig. 2*A*) has a substantial upward trend (0.33 per decade, statistically significant at the 99% confidence level). The dominant spatiotemporal SST variability of ERSST is similar to that of HadISST (Fig. 1*B* and Fig. 2*A*). Thus, the observed SST pattern in the Southern Ocean during the second half of the 20th century is dominated by a broad-scale warming that accounts for one third of the total variance (28% for HadISST and 29% for ERSST). The strongest warming is found in the middle latitudes of the Southern Ocean, and the warming is reduced poleward. Because HadISST and ERSST use different data sources, analysis procedures, and historical bias corrections, the good agreement between them supports confidence in the analyzed Southern Ocean warming during the second half of the 20th century.

Fig. 1*C* shows the first EOF mode of the simulated SST for PIcntrl of CCSM3. For PIcntrl, there is no change in atmospheric composition (i.e., CO_2 is held constant at the preindustrial level), but it includes variations in solar and volcanic forcing and so simulates natural internal variability in response to natural external forcing. The leading EOF mode is characterized by an out-of-phase relationship between the middle and high latitudes, with

Author contributions: J.L. designed research, J.L. performed research, J.L. analyzed data, and J.L. and J.C. wrote the paper.

The authors declare no conflict of interest.

This article is a PNAS Direct Submission.

[1]To whom correspondence should be addressed. E-mail: jliu@eas.gatech.edu.

This article contains supporting information online at www.pnas.org/lookup/suppl/doi:10.1073/pnas.1003336107/-/DCSupplemental.

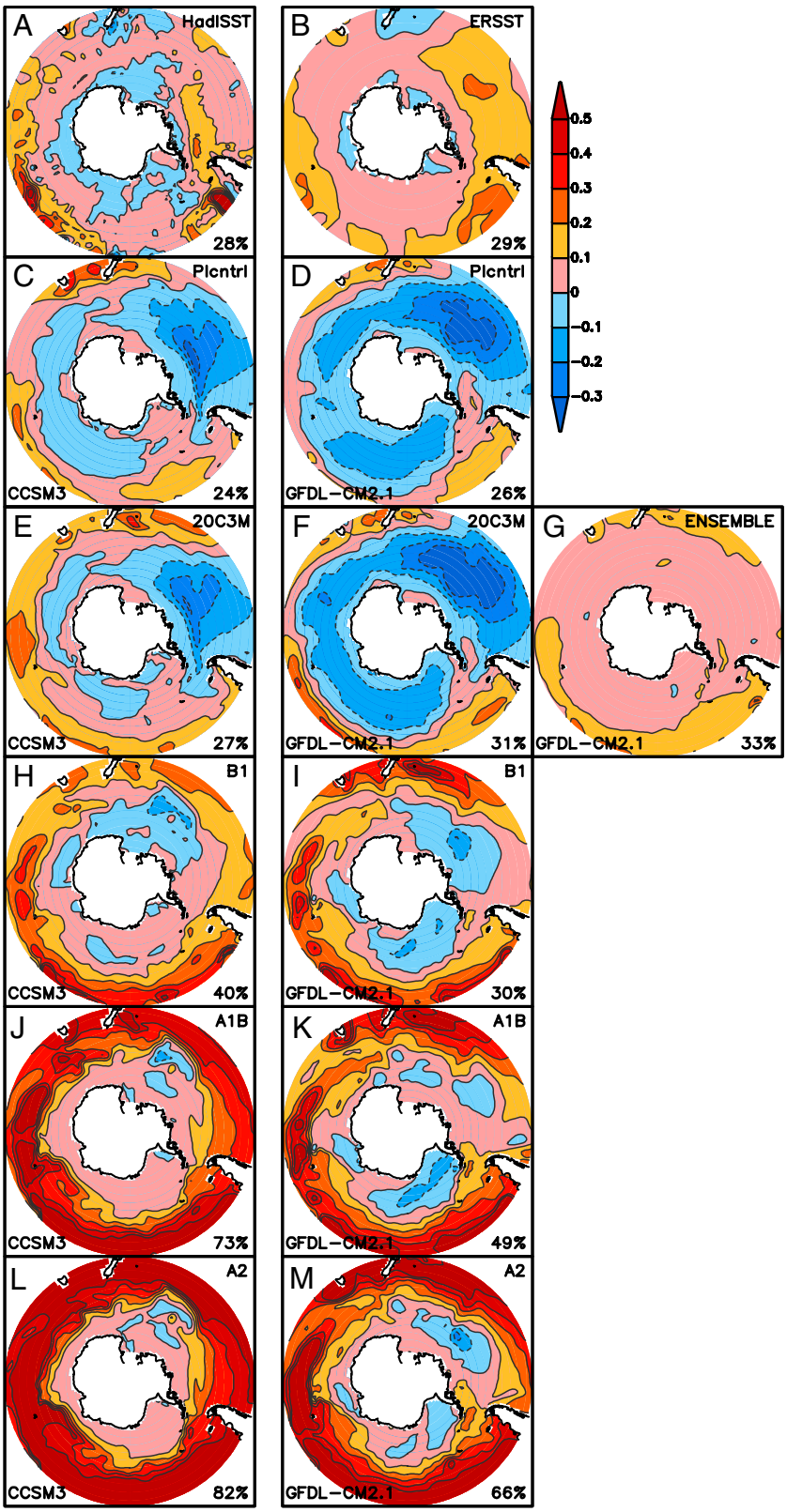

Fig. 1. Spatial patterns of the first EOF mode of the area-weighted annual mean SST south of 40 °S. Observations: (*A*) HadISST and (*B*) ERSST for the period 1950–1999. Simulations of CCSM3 (*Left*) and GFDL-CM2.1 (*Right*): (*C*, *D*) 50-year PIcntrl experiment (natural forcing only), (*E*–*G*) 20C3M experiment for 1950–1999 (anthropogenic and natural forcings), (*H*–*M*) three scenarios (B1, A1B, and A2) for the 21st century.

large SST variability in the eastern south Pacific. The corresponding PC shows large interannual variability, and no significant trend is detected (Fig. 2*B*). The first EOF mode and corresponding PC of the simulated SST for PIcntrl of GFDL-CM2.1 (Fig. 1*D* and Fig. 2*C*) has spatiotemporal variability that is similar to the results of CCSM3.

Many studies suggest that the large-scale atmospheric circulation variability in the Southern Hemisphere is dominated by the

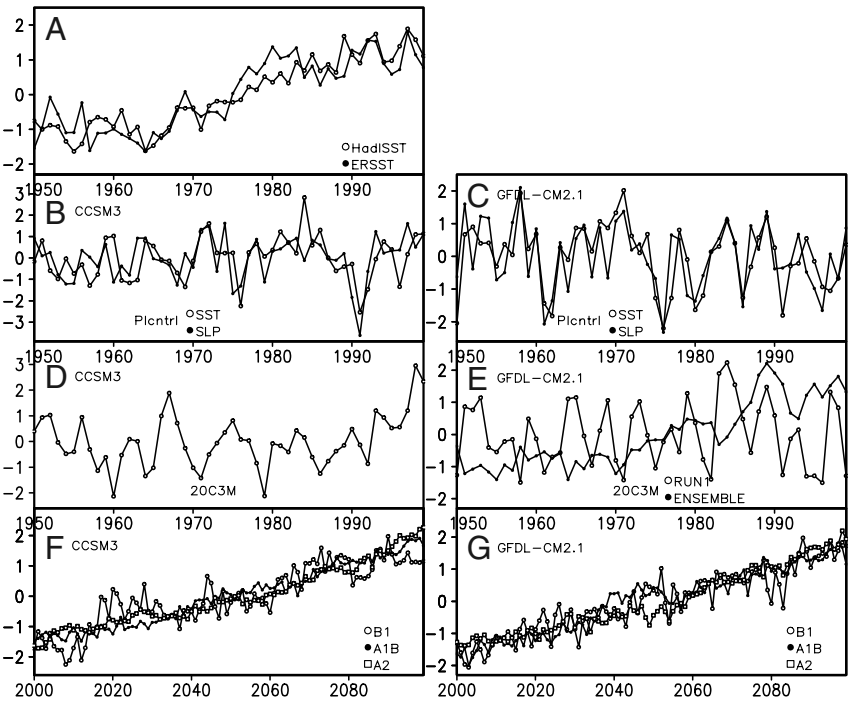

Fig. 2. PCs corresponding to the first EOF modes in Fig. 1: (*A*) HadISST and ERSST, (*B*, *C*) 50-year PIcntrl experiment, (*D*, *E*) 20C3M experiment for 1950–1999, (*F*, *G*) three scenarios (B1, A1B, and A2) for 21st century.

Antarctic Oscillation (AAO). The AAO is characterized by nearly zonally symmetric north-south vacillations in the middle latitude atmospheric westerly jet (13). EOF analysis on the simulated annual-mean sea level pressure (SLP) south of 20 °S for PIcntrl show the correlation between the PCs of the first SLP (representing the AAO) and SST EOF modes is 0.51 for CCSM3 (Fig. 2*B*) and 0.71 for GFDL-CM2.1 (Fig. 2*C*), which are statistically significant at the 99% confidence level. The spatial pattern of SST anomalies associated with the high index polarity of the AAO (warm SST anomalies in the middle latitudes and cold SST anomalies in the high latitudes) bear strong resemblance to the structure of the first SST EOF mode. This indicates that the AAO is the dominant mechanism responsible for the dominant SST variability in the Southern Ocean in the unforced control experiment, which is also consistent with previous observational and modeling studies (14–16).

CCSM3 provides two ensemble members for 20C3M, that is forced with the observed anthropogenic and natural forcings. Rather than the warming pattern found in the observations (Fig. 1*A*), the first EOF modes of the two ensemble members for 20C3M of CCSM3 (Fig. 1*E*, only one run is shown) exhibit spatial variability similar to that of PIcntrl (Fig. 1*C*). The corresponding PCs show strong interannual variability (Fig. 2*D*), which is different from the substantial upward trend found in the observations (Fig. 2*A*). Also, the first EOF modes and corresponding PCs of the five ensemble members for 20C3M of GFDL-CM2.1 (Fig. 1*F* and Fig. 2*E*) resembles its PIcntrl. Thus, none of the models' individual ensemble members have the dominant spatio-temporal SST variability found in the observations that was characterized by the broad-scale warming of the Southern Ocean. If we accept the suite of simulations as a representative sample, the models' internal variability might be too strong (relative to the observations), leading to their deficient response to anthropogenic forcing for the past half century.

We further perform EOF analysis on the averaged SST of the five ensemble members for 20C3M of GFDL-CM2.1, which can be considered as an approximate depiction of the externally forced variability (anthropogenic forcing). The first EOF mode does show a warming pattern in the Southern Ocean present in the observations, and the corresponding PC has an upward trend, though the warming in the middle latitudes of the Southern Ocean for the ensemble mean is weaker than the observations (Fig. 1*G* and Fig. 2*E*).

Over the course of the second half of the 20th century, strong warming in the middle latitudes of the Southern Ocean with weak cooling in the high latitudes is hypothesized here to lead to an enhanced hydrological cycle in the Southern Ocean, whereby evaporation is enhanced and the moisture content of the lower troposphere increases in the middle latitudes of the Southern Ocean. This additional moisture is transported poleward by the meridional circulation (Ferrel Cell), resulting in an increased precipitation, and a freshening of surface water in the high latitudes of the Southern Ocean. To test this hypothesis, a singular value decomposition (SVD) analysis (a method for detecting coupled variability between different components of climate system (17), is performed on the precipitation minus evaporation (P – E), which is obtained from the European Centre for Medium-Range Weather Forecast 40-Year Reanalysis (ERA40)* and HadISST SST south of 40 °S for 1958–1999 to identify the dominant coupled patterns. Fig. 3 shows the spatial patterns and temporal coefficients of the first SVD mode, that accounts for 68% of the total covariance. It appears that the first SVD mode of SST shows spatial pattern that resembles the first SST EOF mode (Fig. 3*A*), and its corresponding temporal coefficients have high correlation (0.92) with the PC of the first SST EOF mode. Associated with the broad-scale warming in the Southern Ocean, the first SVD mode of P – E shows a net freshwater gain in the high latitudes of the Southern Ocean (but extending equatorward into the middle latitudes of the Australian sector) and a net freshwater loss in much of the middle latitudes of the Southern Ocean (Fig. 3*B*). The corresponding time coefficients show a significant upward trend, indicating the hydrological cycle has been enhanced for the latter half of the 20th century

*http://data-portal.ecmwf.int/data/d/era40_moda

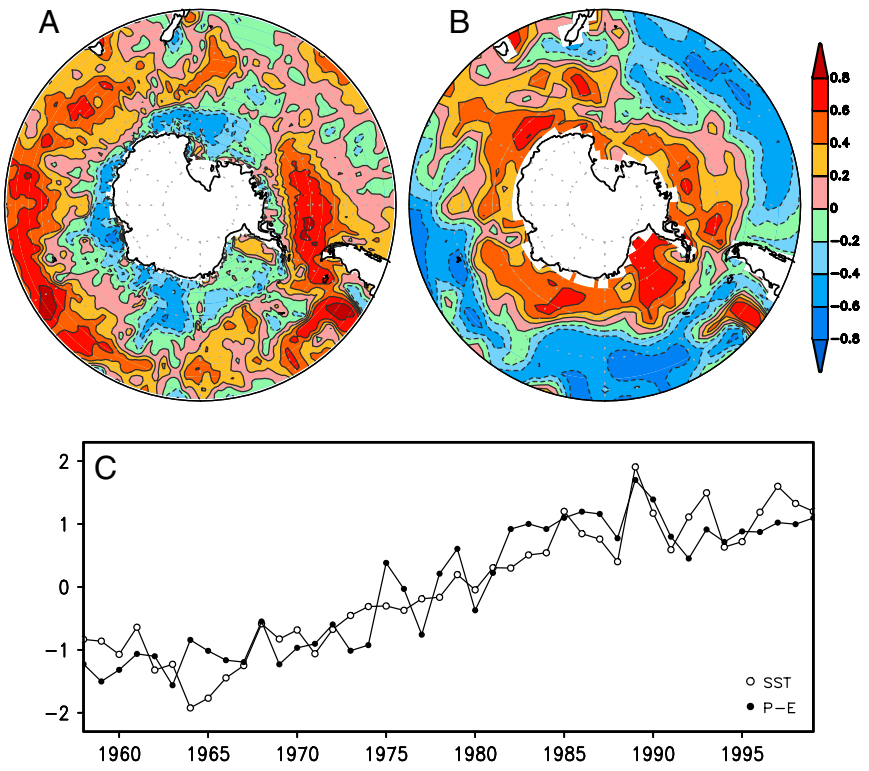

Fig. 3. Spatial patterns of the first SVD mode of the area-weighted annual mean (*A*) HadISST SST and (*B*) ERA40's precipitation minus evaporation, and (*C*) corresponding temporal coefficients for the period 1958–1999.

(Fig. 3*C*). The correlation between the time series of the first SVD mode of P – E and SST is 0.91 for 1958–1999. The satellite-based precipitation of the Global Precipitation Climatology Project also shows an increase (decrease) of precipitation in the high latitudes (much of the middle latitudes) of the Southern Ocean for 1979–1999 (Fig. S1). Furthermore, the hypothesis of the enhanced hydrological cycle in the Southern Ocean is consistent with the findings of previous research (18, 19). Comparisons of historical hydrographic data between 1930 and 1980 with hydrographic data for 1985–1994 showed that the basin wide salinity of the Antarctic Intermediate Water decreases with time. The simplest explanation for this change is a freshening of surface water in the high latitudes of the Southern Ocean, and the estimated increase of P – E in the Southern Ocean is about 31 mm per year between 55° S and 65° S (18). Using measurements from the Argo network of profiling floats and historical oceanographic data, a more-recent analysis detected that the Southern Ocean became fresher since the 1960s, which extends to depths of more than 1,000 m (19). Another potential contributor to the increased freshening of surface water in the southern high latitudes might be the increased melting of glacial ice and iceberg calving.

The increased freshwater input in the high latitudes of the Southern Ocean would decrease the upper ocean salinity (density), leading to a more stable thermohaline stratification and weakened convective overturning. This reduces the upward ocean heat flux available to melt sea ice. Because of the reduced upward ocean heat transport, the simulated SST under sea ice in the 1990s was ~0.2 °C colder than that in the 1950s (Fig. 4*A*). In a weakly stratified Southern Ocean, the ocean heat flux induced ice melt decreases faster than the ice growth, allowing an increase in the net ice production (20). Compared to the 1950s, the simulated total precipitation (liquid precipitation and snowfall) is increased in much of the high latitudes of the Southern Ocean in the 1990s (Fig. 4*E*), which is primarily contributed by the increase of snowfall there (Fig. 4*C*), because the magnitude of the snowfall increase is comparable to that of the total precipitation increase. Also, the differences in the total precipitation and snowfall between the 1990s and 1958–1967 of the ERA40 reanalysis show similar results (Fig. S2). Thus, the increased precipitation in the high latitudes of the Southern Ocean is mainly in a form of snow. This would increase the ice albedo, reducing absorbed solar radiation and encouraging ice growth. As a consequence, the reduced upward ocean heat flux and increased snowfall associated with the enhanced hydrological cycle tends to maintain the Antarctic sea ice, which is consistent with the seeming paradox of the observed increasing total Antarctic sea ice area for the past three decades (0.89×10^5 km^2 per decade; Fig. S3) (21, 22).

The 21st century climate projection experiments conducted by CCSM3 include three emission scenarios, representing low (B1), medium (A1B), and high (A2) increases of CO2 over the course of the 21st century. There is one simulation available for each of the B1 and A2 scenarios, but four ensemble members for the A1B scenario. Fig. 1 *H*, *J*, and *L* and Fig. 2*F* show the EOF analyses of the projected SST during the 21st century for CCSM3. The first EOFs of all three scenarios show warming for much of the Southern Ocean, although weak cooling exists in the central South Pacific. This pattern is different from the dominant SST pattern present in the two ensemble members of 20C3M. Furthermore, the warming of the Southern Ocean becomes much stronger, particularly in the ACC, from low (B1), through medium (A1B), to high (A2) emissions. Larger positive values in the EOFs mean stronger warming, given that the magnitude of the trend for the PCs (0.31, 0.34, 0.34 per decade for B1, A1B, A2, respectively) is almost the same for the three scenarios. Also, the total variance explained by the warming pattern is doubled from low (40% for B1) to high (82% for A2) emissions, and can be as large as 91% for the ensemble mean of A1B. The EOF analysis of the three emission scenarios for GFDL-CM2.1 is in good agreement with the results of CCSM3 (Fig. 1 *I*, *K*, and *M* and Fig. 2*G*), although the GFDL-CM2.1 shows weak cooling in the Southern Atlantic, and the percentage of variance explained differs somewhat between the two sets of model simulations. This suggests

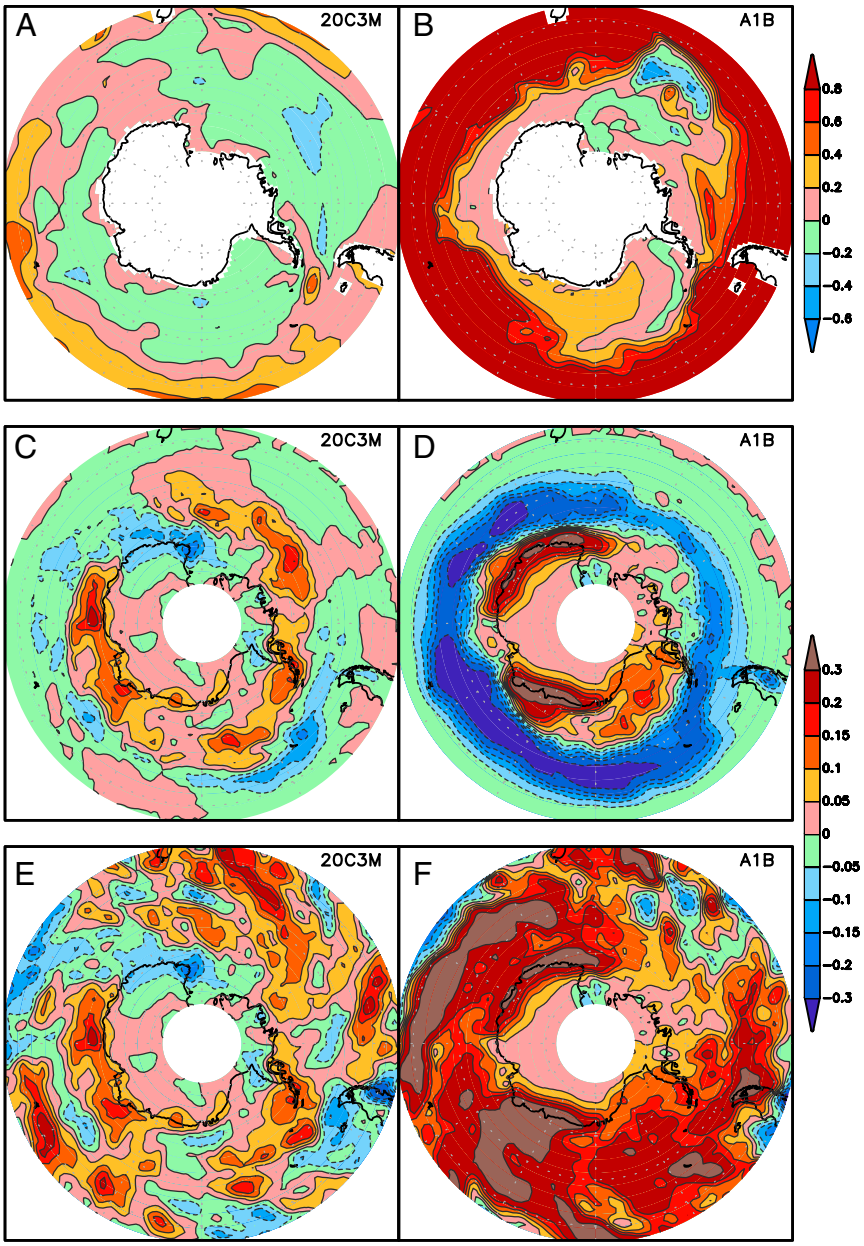

Fig. 4. Differences in sea surface temperature (°C, *Upper*), snowfall (mm/day, *Center*) and total precipitation (mm/day, *Lower*): (*A*) between the 1990s and 1950s for 20C3M of CCSM3, and (*B*) between the 2090s and 2000s for A1B of CCSM3.

that impacts of anthropogenic forcing become strong enough to overwhelm the dominant mode of natural internal variability (AAO) present in the models during the 21st century, even for the low emission scenario.

Discussion

With increased loading of greenhouse gases through the 21st century, the models suggest that there is an accelerated warming in the Southern Ocean. Moreover, there is a strong poleward expansion of the warming from low to high emissions (Fig. 1 *D–F*). As shown in Fig. 4*B*, SST under sea ice in the 2090s is a few tenths degree warmer than that in the 2000s, and the warming could be as large as ~1–1.5 °C in the ACC. Thus, the pronounced warming in the Southern Ocean during the 21st century offsets and exceeds the cooling effect associated with the decrease of upward ocean heat transport as a result of the enhanced hydrological cycle. As the warming extends poleward, the circumpolar westerlies are projected to intensify and shift poleward due to increasing greenhouse gases, coupled with the presence of the Antarctic ozone hole (1). The storm track as indicated by transient eddy kinetic energy also increases in magnitude and shifts poleward and upward (23). This allows more heat and moisture to be transported poleward by the atmosphere, resulting in an increasing tendency of liquid precipitation, rather than snow, in the high latitudes of the Southern Ocean. As shown in Fig. 4*D*, the region covered with increased snowfall retreats to around the Antarctic continent in the 2090s as compared to the 2000s. At the same time, there is an increase of the total precipitation (liquid precipitation + snowfall) for much of the Southern Ocean, particularly in the high latitudes of the Southern Ocean (Fig. 4*F*). This suggests increased liquid precipitation in 55° S–65° S (particularly in the marginal sea ice zone) associated with the enhanced hydrological cycle. Liquid precipitation promotes surface melt of snow and ice, which also reduces the surface albedo, lead-

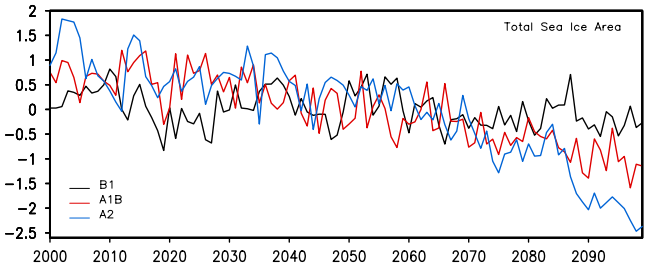

Fig. 5. Time series of the total Antarctic sea ice area anomaly ($\times 10^5$ km^2) for the three scenarios during the 21st century.

ing to more absorbed solar radiation. Because of increased heating from below (ocean) and above (atmosphere), combined with increased liquid precipitation, the Antarctic sea ice is expected to decline in the 21st century. As shown in Fig. 5, all three scenarios show a loss of the total Antarctic sea ice area over the 21st century (0.4×10^5 km^2 per decade for B1, 2×10^5 km^2 per decade for A1B, and 3.02×10^5 km^2 per decade for A2), with the greatest loss occurring in the Atlantic and Indian sectors of the Antarctic. Additionally, the rate of decline accelerates after the late 2060s for the A1B and A2 scenarios. Thus, improved representation in models of atmosphere–sea ice–ocean interactions will be critical for forecasting Antarctic sea ice changes as climate warms.

Methods

The observed SST datasets used in the study include the Hadley Centre Sea Ice and Sea Surface Temperature (7), and the extended reconstructed sea surface temperature (8) for 1950–1999. Precipitation and evaporation obtained from the European Centre for Medium-Range Weather Forecast 40-Year Reanalysis* for 1958–1999, and Antarctic sea ice index obtained from the National Snow and Ice Data Center† are used to facilitate the analysis. We use model outputs from (*i*) the NCAR Community Climate System Model 3.0, and (*ii*) the Geophysical Fluid Dynamics Laboratory Coupled Climate Model, including the preindustrial control experiment, the climate of the 20th century experiment, and the 21st century climate projection experiments. We identify the dominant spatial and temporal patterns of SST variability in the Southern Ocean using EOF analysis. The EOF mode identifies regions that are closely related and with strong gradient (spatial variability), and the PC indicates the amplitude of EOF as it varies through time (temporal variability). Here, we focus on the first EOF modes that are statistically significant (24). We use the singular value decomposition analysis to identify the dominant coupled pattern between the ERA40's precipitation minus evaporation and HadISST SST south of 40 °S for 1958–1999.

ACKNOWLEDGMENTS. We thank the Program for Climate Model Diagnosis and Intercomparison for collecting and archiving model outputs for the Fourth Assessment of the Intergovernmental Panel on Climate Change. This research was supported by the National Sciene Foundation Polar Programs (0838920) and National Aeronautics and Space Administration (NASA) Energy and Water Cycle Study (NEWS).

†http://nsidc.org/data/g02135.html

1. Mayewski PA, et al. (2009) State of the Antarctic and Southern Ocean climate system. *Rev Geophys* 47:RG1003 doi: 10.1029/2007RG000231.
2. Hegerl GC, Bindoff NL (2005) Warming of the world's oceans. *Science* 309:254–255.
3. Levitus S, Antonov JL, Boyer TP (2005) Warming of the world ocean. 1955–2003. *Geophys Res Lett* 32:L02604 doi: 10.1029/2004GL021592.
4. Gille S (2008) Decadal-scale temperature trends in the Southern Hemisphere Ocean. *J Climate* 21:4749–4765.
5. Wainer I, Taschetto A, Otto-Bliesner B, Brady E (2004) A numerical study of the impact of greenhouse gases on the South Atlantic Ocean climatology. *Climatic Change* 66:163–189.
6. Fyfe JC (2006) Southern Ocean warming due to human influence. *Geophys Res Lett* 33 doi: 10.1029/2006GL027247.
7. Rayner NA, et al. (2003) Global analyses of sea surface temperature, sea ice, and night marine air temperature since the late nineteenth century. *J Geophys Res* 108 doi: 10.1029/2002JD002670.
8. Smith TM, Reynolds RW (2004) Improved extended reconstruction of SST (1854–1997). *J Climate* 17:2466–2477.
9. Smith TM, Reynolds RW (2003) Extended reconstruction of global sea surface temperatures based on COADS data (1854–1997). *J Climate* 16:1495–1510.
10. Raphael M, Holland M (2006) Twentieth century simulation of the southern hemisphere climate in coupled models. Part I: Large scale circulation variability. *Clim Dynam* 26:217–228.
11. Holland M, Raphael M (2006) Twentieth century simulation of the southern hemisphere climate in coupled models. Part II: Sea ice conditions and variability. *Clim Dynam* 26:229–245.
12. Russell JL, Souffer RJ, Dixon KW (2006) Intercomparison of the Southern Ocean Circulations in the IPCC Coupled Model Control Simulations. *J Climate* 19:4560–4575.
13. Thompson DWJ, Wallace JM (2000) Annular modes in the extratropical circulation. Part I: Month-to-month variability. *J Climate* 13:1000–1016.
14. Hall A, Visbeck M (2002) Synchronous variability in the Southern Hemisphere atmosphere, sea ice, and ocean resulting from the annular mode. *J Climate* 15:3043–3057.
15. Sen Gupta A, England MH (2006) Coupled ocean-atmosphere-ice response to variations in the Southern Annular Mode. *J Climate* 19:4457–4486.
16. Ciasto LM, Thompson DWJ (2008) Observations of large-scale ocean–atmosphere interactions in the Southern Hemisphere. *J Climate* 21:1244–1259.
17. Bretherton CS, Smith C, Wallace JM (1992) An intercomparison of methods for finding coupled patterns in climate data. *J Climate* 5:541–560.
18. Wong APS, Bindoff NL, Church JA (1999) Large-scale freshening of intermediate waters in the Pacific and Indian Oceans. *Nature* 400:440–443.
19. Boning CW, Dispert A, Visbeck M, Rintoul SR, Schwarzkopf FU (2008) The response of the Antarctic circumpolar current to recent climate change. *Nat Geosci* 1:864–869.
20. Zhang J (2007) Increasing Antarctic sea ice under warming atmospheric and oceanic conditions. *J Climate* 20:2515–2529.
21. Liu J, Curry JA, Martinson DG (2004) Interpretation of recent Antarctic sea ice variability. *Geophys Res Lett* 31:L02205 doi: 10.1029/2003GL018732.
22. Cavalieri DJ, Parkinson CL (2008) Antarctic sea ice variability and trends. 1979–2006. *J Geophys Res* 113:C07004 doi: 10.1029/2007JC004564.
23. Yin JH (2005) A consistent poleward shift of the storm tracks in the simulations of 21st century climate. *Geophys Res Lett* 32:L18701 doi: 10.1029/2005GL023684.
24. North GR, Bell TL, Cahalan RF, Moeng FJ (1982) Sampling errors in the estimation of empirical orthogonal functions. *Mon Weather Rev* 110:699–706.